

TransDiffuser: End-to-end Trajectory Generation with Decorrelated Multi-modal Representation for Autonomous Driving

Xuefeng Jiang^{1,2} Yuan Ma^{1,3} Pengxiang Li^{1,3} Leimeng Xu¹ Xin Wen¹
 Kun Zhan^{1*} Zhongpu Xia¹ Peng Jia¹ Xianpeng Lang¹ Sheng Sun^{2*}

¹LiAuto ²Institute of Computing Technology, Chinese Academy of Sciences ³Tsinghua University
 jiangxuefeng21b@ict.ac.cn, zhankun@lixiang.com, sunsheng@ict.ac.cn

Abstract: In recent years, diffusion model has shown its potential across diverse domains from vision generation to language modeling. Transferring its capabilities to modern autonomous driving systems has also emerged as a promising direction. In this work, we propose TransDiffuser, an encoder-decoder based generative trajectory planning model for end-to-end autonomous driving. The encoded scene information serves as the multi-modal conditional input of the denoising decoder. To tackle the mode collapse dilemma in generating high-quality diverse trajectories, we introduce a simple yet effective multi-modal representation decorrelation optimization mechanism during the training process. TransDiffuser achieves PDMS of 94.85 on the NAVSIM benchmark, surpassing previous state-of-the-art methods without any anchor-based prior trajectories.

Keywords: End-to-end Autonomous Driving, Representation Learning

1 Introduction

Autonomous driving [1, 2] has gained widespread attention from both academia and industry for its potential in improving traffic safety and efficiency. Substantial advancements have been attained across a diverse range of tasks, including real-time localization [3, 4], scene perception [5, 2] and motion planning [6]. Early motion planning methods typically involve a sequential process of perception, prediction, and subsequent planning, which leads information loss and cascading latency [7]. In recent years, an important research direction is to develop planning-oriented autonomous driving systems [1] in a fully end-to-end manner. With raw sensor data as input, an end-to-end driving model is expected to directly output a desirable trajectory to guide future motion planning. Early works [1, 8] aim to produce a single plausible trajectory by merely imitating the annotated human expert driving behaviors in the training dataset.

However, this data-driven paradigm may not be fully capable to generalize to the real-world scenarios. Considering the existence of diverse yet complex driving scenarios and different feasible driving styles [9], there is rarely only one feasible trajectory [10]. Recent attempts [11, 12, 13, 10] have increasingly focused on generating multi-mode future trajectories as feasible candidates². To generate multi-mode high-quality trajectories from the continuous action space, one research line, represented by HydraMDP series [13, 14, 15], simplifies this challenge into selecting most feasible candidates from a fixed planning vocabulary to discretize the action space. Another notable research trend [10, 16, 9]

*Corresponding Authors.

²In this paper, *multi-mode trajectories* denote generating multiple possibly feasible candidate trajectories.

aims to transfer the success of diffusion models [17] in robotics domain [18] to generate multi-mode trajectories in end-to-end autonomous driving domain, using scene and motion information as conditional input to produce multi-mode trajectories as candidates. Similar to Hydra-MDP series, GoalFlow [10] imposes a strong constraint on the trajectory generation process by establishing a dense vocabulary of anchor trajectory endpoints. DiffusionDrive [16] further highlights the issue of mode collapse, wherein the generated trajectories lack diversity, as different random noise inputs tend to converge to similar trajectories during the denoising process. Therefore, it implements a truncating diffusion policy by partitioning the Gaussian distribution into multiple sub-Gaussian distributions centered around prior anchor trajectories.

Following the intuition of the above recent Diffusion based approach, we propose TransDiffuser, an encoder-decoder based multi-mode trajectory generation model. We utilize the frozen Transfuser backbone [8] to encode the scene perception information. Then, the scene information from front-view cameras and LiDAR, and motion information of the current ego vehicle is encoded as the conditional input of the Diffusion based denoising decoder. Unlike previous works, we identify another underlying bottleneck that leads to mode collapse in generated trajectories: The under-utilization of the encoded multi-modal conditional information. To generate more diverse feasible trajectories, we introduce a computation-efficient yet effective plug-and-play multi-modal representation decorrelation optimization mechanism during the denoising process, which aims to better exploit the multi-modal representation space to guide more diverse feasible planning trajectories from the continuous action space. As a result, the proposed method achieves the new state-of-the-art performance on the planning-oriented NAVSIM benchmark without any explicit guidance like anchor-based trajectories. To sum up, our contributions can be summarized as follows:

- We propose an encoder-decoder generative trajectory model TransDiffuser. It firstly encode the scene perception and motion of the ego vehicle, and then utilize the encoded information as conditional input of Denoising Decoder to decode multi-mode diverse feasible trajectories.
- To further increase the diversity of generated trajectories, we introduce a computation-efficient multi-modal representation decorrelation mechanism during the training process.
- We achieve the new state-of-the-art PDM score 94.85 on the NAVSIM benchmark without any explicit guidance like anchor trajectories or predefined vocabulary.

2 Related Works

2.1 End-to-end Autonomous Driving

Modern autonomous driving systems [1, 16, 12, 13, 9] increasingly adopt end-to-end learning paradigms to directly map raw sensor data to driving decisions, streamlining the process from perception to action. Herein we review most recent advances in end-to-end autonomous driving for motion planning task. We categorize current methods into three groups as shown in Table 1.

Auto-regressive Based Models. This approach is relatively traditional, which typically predict a trajectory via sequential Auto Regressive (AR) generating. To our best knowledge, UniAD [1] is the pioneering work showcasing the potential of end-to-end autonomous driving by integrating multiple perception tasks to facilitate planning. Transfuser [8] integrates image and LiDAR representations using self-attention mechanism and uses GRU to yield the planning trajectory in an auto-regressive paradigm. Its variant, LTF, is a light-weight image-only version where the LiDAR backbone is replaced by a learnable embedding. PARA-Drive [19] proposes a computationally efficient system which performs mapping, planning, motion prediction, and occupancy prediction tasks in parallel.

Scoring Based Models. This approach often generates multi-mode trajectories and selects optimal trajectory with the designed scoring functions. VADv2 [12] is an early attempt to perform multi-mode planning by scoring and sampling from a large fixed vocabulary of anchor trajectories. Centaur [20] employs cluster entropy to measure uncertainty by analyzing the distribution of multiple trajectory candidates generated by the planner. WoTE [21] leverages a latent BEV world model to forecast

future BEV states for trajectory evaluation. Hydra-MDP series [13, 14, 15] convert the trajectory generation task into selecting optimal trajectory from predefined trajectory vocabulary. and propose an expert-guided hydra distillation strategy to align the planner with simulation-based metrics.

Diffusion Based Models. GoalFlow [10] employs flow matching to generate goal-conditioned, multi-mode trajectories and introduces a trajectory scorer to efficiently select optimal trajectory using the goal point as a reference. DiffusionDrive [16] uses truncated diffusion policy to address the issues of mode collapse and reduce heavy computational overhead by denoising from anchored Gaussian distributions (\dagger in Table 1) instead of anchor trajectories with fewer steps while preserving trajectory diversity. TrajHF [9] pioneers to introduce additional reinforcement learning on their private dataset to fine-tune the generative trajectory model.

Table 1: Comparison of existing models. * denotes generating multi-mode candidate trajectories.

Model	Venue	Year	Image Encoder	LiDAR	Anchor	Paradigm
Transfuser [8]	ICRA & TPAMI	2023	ResNet-34	✓	–	AR
UniAD [1]	CVPR	2023	ResNet-34	–	–	AR
PARA-Drive [19]	CVPR	2024	ResNet-34	–	–	AR
VADv2 [12]	–	2024	ResNet-34	–	✓	Scoring*
Hydra-MDP [13]	CVPRW	2024	ResNet-34	✓	✓	Scoring*
DiffusionDrive [16]	CVPR	2025	ResNet-34	✓	✓ \dagger	Diffusion*
GoalFlow [10]	CVPR	2025	ResNet-34	✓	✓	Diffusion*
Hydra-MDP++ [14]	–	2025	ResNet-34	–	✓	Scoring*
Hydra-NeXt [15]	–	2025	ResNet-34&V2-99	–	✓	Scoring*
TrajHF [9]	–	2025	ViT	✓	–	Diffusion*
Centaur [20]	–	2025	ResNet-34	✓	✓	Scoring*
WoTE [21]	–	2025	ResNet-34	✓	✓	Scoring*
TransDiffuser (Ours)	–	2025	ResNet-34	✓	–	Diffusion*

2.2 Generative Trajectory Model

Generative models have garnered significant attention in both academic and industry due to their remarkable capabilities in producing realistic data across various domains. These models have been successfully applied in numerous tasks, such as image synthesis using Generative Adversarial Network [22] and Variational Autoencoder [23], text generation with large language models [24], and audio synthesis with WaveNet [25]. Diffusion models have been proposed and widely studied in recent years, and demonstrated their powerful generative abilities across vision generation [17, 26, 27, 28] and language generation [29]. A recent shift has emerged in the field of end-to-end autonomous driving, where researchers [16, 10, 9] embark on exploring the use of Diffusion models for planning tasks. Diffusion models, known for their ability to generate high-quality data by iteratively denoising random noise, have shown promise in generating smooth and realistic driving trajectories. However, pointed by DiffusionDrive [16], one bottleneck for diffusion models is that diffusion based trajectory generative models showcases the less diversity of the decoded denoised trajectories. *This issue is often called by mode collapse.* It proposes truncated diffusion policy that begins the denoising process from an anchored gaussian distribution instead of a standard Gaussian distribution. GoalFlow [10] used a goal point vocabulary to mitigate the mode collapse issue to assist the efficient trajectory generation. Different from above works, we aim to mitigate the mode collapse issue via improving the fused intermediate multi-modal representations, which assists to increase the diversity of final decoded trajectories. Notably, we do not utilize any form of guide information such as anchors or vocabulary, allowing for more flexible and diverse planning.

2.3 Representation Learning

Representation learning has shown its potential in many deep learning applications like self-supervised learning [30], supervised classification [31, 32, 33], noisy label learning [34, 35, 36] and reinforcement learning [37]. In general, these attempts aim to fully exploit the representation space to learn better intermediate representations for downstream applications. One popular approach is contrastive learning [38, 39] by mining the representation similarities among positive and negative examples. However, this approach generally requires very large training batch (e.g. 4096 or 8192) to fully extract

reliable supervision from batch examples, which may be not suitable and computation-efficient for training autonomous driving models. Inspired by recent representation learning works [37, 34, 31, 40], we optimize the intermediate representations in our task by decoupling the interactions of different representation dimensions. This optimization approach does not rely on the large training batchsize and bring little computation overhead as analyzed in [37, 31], which we will introduce in Section 3.4.

3 Method

3.1 Preliminary

As shown in Fig. 1, our framework is generally an encoder-decoder model, which consists of two main components: Scene Encoder and Denoising Decoder. It takes raw sensor data as input and predicts the future trajectory by accumulating consequent decoded actions. The derived trajectory is represented as a sequence of waypoints (states) $x = \{s_1, s_2, \dots, s_{\mathcal{T}}\}$, where \mathcal{T} denotes the trajectory length, and each state s_{τ} is the location of the τ -th waypoint in the current driving agent’s ego-centric coordinate system. Following [9], each waypoint can connect to its neighbor waypoints by sequentially projecting to action space to mitigate heteroscedasticity along the trajectory timeline. The projection can be recursively expressed as:

$$\hat{x}_{\tau}, \hat{x}_1 = s_{\tau} - s_{\tau-1}, s_1 \quad (1)$$

where \hat{x}_{τ} represents the agent’s action at timestep τ , and τ ranges from 2 to \mathcal{T} . This mapping guarantees a reversible connection between the two spaces. As a result, the trajectory can be easily deduced through the accumulation of actions.

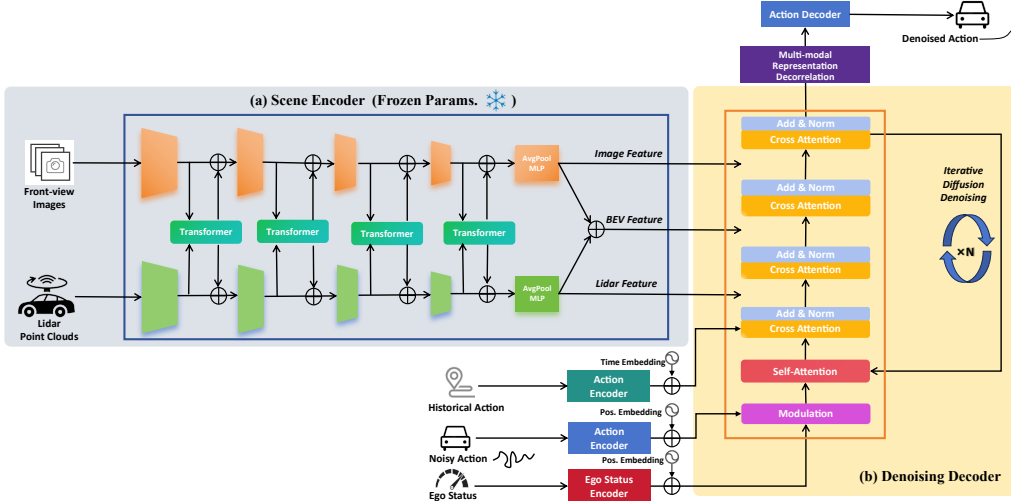


Figure 1: Overview of the proposed TransDiffuser architecture. Note that the parameters of the scene perception (images and LiDAR) encoder are frozen.

3.2 Scene & Motion Encoder

We utilize a Scene Encoder (Figure 1(a)) based on the Transfuser backbone [8], pre-trained on Nav-train, to process rich perception information from front-view cameras and LiDAR sensors. This multi-modal approach is crucial as single modalities often lack essential environmental details. Image and LiDAR information are processed through separate backbone networks (dependent branches). We perform multi-stage fusion by connecting features from corresponding stages of both branches via Transformer blocks [41]. This allows for cross-modal attention, leading to enhanced multi-scale representations and better overall integration of sensor data. The final output of Scene Encoder include the image feature F_{img} , LiDAR feature F_{LiDAR} and BEV feature F_{bev} .

To provide essential motion context for predicting future actions, the encoder processes two types of motion information. Firstly, the historical ego trajectory is encoded into an action embedding

Emb_{action} using a dedicated Multi-Layer Perceptron (MLP), referred to as the Action Encoder. Secondly, the current ego vehicle status is encoded into an ego status embedding Emb_{ego} by another MLP (Ego Status Encoder). Following [9], these two motion-related embeddings are designed to be utilized within the Denoising Decoder. The encoded scene and motion feature group $feat = \{F_{bev}, F_{img}, F_{LiDAR}, Emb_{action}, Emb_{ego}\}$ is the conditional input of our Denoising Decoder.

3.3 Denoising Decoder

The Denoising Decoder (Figure 1(b)) is responsible for generating the planned trajectory by iteratively refining an initial noise estimate, conditioned on the encoded scene and motion features derived from the Scene Encoder. It takes the encoded feature group $feat = \{F_{bev}, F_{img}, F_{LiDAR}, Emb_{action}, Emb_{ego}\}$ as conditional input. Different features within this group are sequentially fused via multi-head cross-attention [41]. The decoder then outputs a feasible action from the continuous action space. By periodically accumulating these decoded actions, the final trajectory is formed.

To achieve this generation and handle the complexity of driving scenarios, we employ Denoising Diffusion Probabilistic Models (DDPM) [17] as the optimization framework. DDPM involves forward process where noise is gradually added to the ground truth data, and reverse process where the model learns to denoise. Following [9, 16], we focus on reverse denoising process, which transitions from Gaussian noise towards noise-free state x_0 . This transition is governed via this equation:

$$x_{t-1} = \frac{1}{\sqrt{\alpha_t}}(x_t - \frac{1 - \alpha_t}{\sqrt{1 - \bar{\alpha}_t}}\epsilon_\theta(x_t, t, feat)) + \sigma_t z \quad (2)$$

where $z \sim \mathcal{N}(0, I)$, $t \in \{1, \dots, \mathbf{T}\}$ denotes the noise level timestep, \mathbf{T} is the total number of denoising steps, and ϵ_θ represents our denoising decoder parameterized by θ . The noise prediction ϵ_θ is conditioned on the noisy state x_t , the timestep t , and the feature group $feat$. The parameters $\alpha_t = 1 - \beta_t$, $\bar{\alpha}_t = \prod_{i=1}^t \alpha_i$, and $\sigma_t^2 = \beta_t$ are derived from a predefined noise schedule β_t . Essentially, Equation 2 describes how to estimate a slightly less noisy state (x_{t-1}) from the current noisy state (x_t) using the model's noise prediction (ϵ_θ).

The decoder is trained to accurately predict the noise added during the forward process. The optimization objective involves minimizing the difference between the actual sampled noise ϵ and the predicted noise ϵ_θ , formulated as a gradient descent step on:

$$\nabla_\theta ||\epsilon - \epsilon_\theta(\sqrt{\alpha_t}x_0 + \sqrt{1 - \bar{\alpha}_t}\epsilon, t, feat)||^2 \quad (3)$$

where ϵ is randomly sampled from $\mathcal{N}(0, I)$. The detailed computation of this trajectory denoising loss, \mathcal{L}_{diff} , using Mean Squared Error (MSE) is outlined in Algorithm 1.

Algorithm 1: The computation process of trajectory denoising loss \mathcal{L}_{diff}

Input: Trajectory GT $label$, Scene feature $feat$, Number of denoising timesteps \mathbf{T}

Output: Trajectory loss \mathcal{L}_{diff}

- 1 $noise \leftarrow \text{Gaussian}(label.shape)$; // Generate random Gaussian noise
 - 2 $step \leftarrow \text{Rand}(0, \mathbf{T})$; // Pick a random time step
 - 3 $noisy_target \leftarrow \text{AddNoise}(label, noise, step)$; // Apply noise in the forward process
 - 4 $pred \leftarrow \text{Denoising_Decoder}(noisy_target, step, feat)$; // Denoising process
 - 5 $\mathcal{L}_{diff} \leftarrow \text{MSE}(pred, noise)$;
 - 6 **return** \mathcal{L}_{diff} ;
-

During the inference process, the model leverages this learned denoising process to generate a pool of diverse candidate trajectories starting from pure noise. In our implementation, we generate 30 candidates considering efficiency. Subsequently, a rejection sampling [9] strategy is employed to filter out dynamically infeasible or unsuitable trajectories. This contrasts with methods like GoalFlow [10] generating 128/256 candidates or TrajHF [9] using 100 candidates before selection or filtering. This reflects the inference efficiency of our method.

3.4 Multi-modal Representation Decorrelation

The final denoised action is decoded by the action decoder as illustrated in Figure 2. We believe that the final performance is largely determined by the quality of the learned multi-modal fused representations. To tackle this information bottleneck [42], we apply multi-modal representation optimization objective on the fused multi-modal representations, which is illustrated in Figure 2. In detail, the input multi-modal representation matrix \mathbf{M} (shown in Figure 1) with shape $\mathbf{B} \times \mathbf{D}$, where \mathbf{B} and \mathbf{D} denote the batchsize and the reshaped multi-modal representation dimension of each sample. Detailedly, in our implementation, \mathbf{M} is reshaped from $B \times 8 \times 256$ to $B \times 2048$. We first normalize multi-modal representation matrix \mathbf{M} and then compute its correlation matrix **corr**. This penalty \mathcal{L}_{reg} is designed to decrease non-diagonal entries of the multi-modal correlation matrix **corr**.

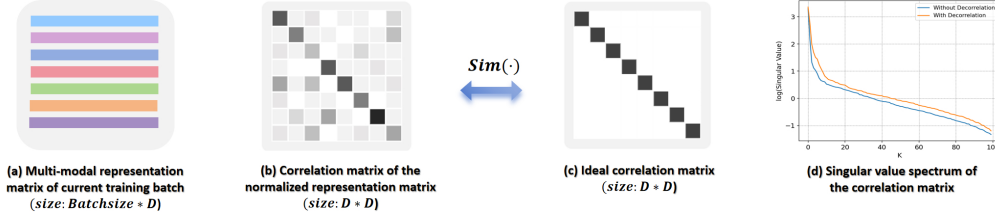


Figure 2: Illustrations on the multi-modal representation decorrelation process. (d) shows top 100 largest singular values of the correlation matrices. We observe the proposed decorrelation mechanism helps to better utilize the representation space before action decoding (shown in Figure 1).

Intuitively, \mathcal{L}_{reg} aims to regularize the multi-modal correlation matrix (i.e. Figure 2) to be similar to the diagonal form. This can be achieved by eliminating the unnecessary interactions of different dimensions of representation to increase the similarity (illustrated as $\text{sim}(\cdot)$) to identity matrix or diagonal matrix (i.e. Figure 2(c)). As the figure shows, the derived \mathcal{L}_{reg} is a batch-level regularization objective which optimizes the multi-modal representations in each training batch. Since the singular values of the covariance matrix **corr** provide a comprehensive characterization [31] of the distribution of multi-modal representations \mathbf{M} , we visualize the largest singular values shown in Figure 2(d). We also provide the batch-level sensitivity study in Section 4.3.

Algorithm 2: The computation process of \mathcal{L}_{reg}

Input: Reshaped Multi-modal representation matrix \mathbf{M}

Output: \mathcal{L}_{reg}

- 1 $\mathbf{M}, \sigma_{\mathbf{M}} \leftarrow \mathbf{M} - \text{Mean}(\mathbf{M}, \text{keepdim} = \text{True}), \text{Var}(\mathbf{M}, \text{keepdim} = \text{True})$;
 - 2 $\mathbf{M} \leftarrow \frac{\mathbf{M}}{\sqrt{\epsilon + \sigma_{\mathbf{M}}}}$; //Normalization. $\epsilon = 1e^{-8}$ is used to avoid zero denominator.
 - 3 **corr** $\leftarrow \mathbf{M}^T \cdot \mathbf{M}$; //Compute the correlation matrix.
 - 4 **côrr** $\leftarrow \text{remove_diagonal_elements}(\mathbf{corr})$; //Extract the non-diagonal elements.
 - 5 $\mathcal{L}_{reg} \leftarrow (\mathbf{côrr}^2.\text{mean}()) / \mathbf{B}$;
 - 6 **return** \mathcal{L}_{reg} ;
-

During the training process, we combine the supervised \mathcal{L}_{diff} and the multi-modal representation decorrelation loss with the trade-off coefficient β to form the overall optimizing objective:

$$\mathcal{L} = \mathcal{L}_{diff} + \beta \mathcal{L}_{reg}. \quad (4)$$

4 Experiments

4.1 Experimental Setup

Dataset. We utilize the well-established planning-oriented NAVSIM dataset [43] using non-reactive simulation and closed-loop evaluations. It builds on the existing OpenScene [44] dataset, a compact version of nuPlan [45] sampled at 2 Hz. Each sample contains camera images from 8 perspectives,

Table 2: Performance on Navtest with closed-loop metrics. **L**, **V** and **V*** denote the LiDAR input, vision input, and the video or historical image frame input, respectively.

Method	Modality	Metrics					
		$NC \uparrow$	$DAC \uparrow$	$EP \uparrow$	$TTC \uparrow$	$C \uparrow$	$PDMS \uparrow$
Constant Velocity [43]	-	68.0	57.8	19.4	50.0	100.0	20.6
Ego Status MLP [43]	-	93.0	77.3	62.8	83.6	100.0	65.6
Transfuser [8]	V+L	97.8	92.6	78.9	92.9	100.0	83.9
LTF [8]	V	97.4	92.8	79.0	92.4	100.0	83.8
UniAD [1]	V+L	97.8	91.9	78.8	92.9	100.0	83.4
PARA-Drive [19]	V*+L	97.9	92.4	79.3	93.0	99.8	84.0
DiffusionDrive [16]	V+L	98.2	96.2	82.2	94.7	100.0	88.1
GoalFlow [10]	V+L	98.4	98.3	85.0	94.6	100.0	90.3
VADv2 [12]	V+L	97.2	89.1	76.0	91.6	100.0	80.9
Hydra-MDP [13]	V+L	99.1	98.3	85.2	96.6	100.0	91.3
Hydra-NeXt [15]	V	98.1	97.7	81.8	94.6	100.0	88.6
Hydra-MDP++ (ResNet34) [14]	V*	97.6	96.0	80.4	93.1	100.0	86.6
WoTE [21]	V+L	98.5	95.8	80.9	94.4	99.9	87.1
Hydra-MDP++ (V2-99) [14]	V*	98.6	98.6	85.7	95.1	100.0	91.0
Centaur [20]	V+L	99.5	98.9	85.9	98.0	100.0	92.6
TrajHF [9]	V+L	99.3	97.5	90.4	98.0	99.8	94.0
TransDiffuser (Ours)	V+L	99.4	96.5	94.1	97.8	99.4	94.9

fused LiDAR data from 5 sensors, ego status, and annotations for the map and objects. It has two parts: Nav-train and Nav-test, which respectively contain 1192 and 136 scenarios for training/validation and testing, and we only use the training split for training and validation set to guide model selection.

Baseline. In this work, we compare the proposed framework against counterparts from three groups discussed in Section 2. Following [43, 10], we additionally refer to *Constant Velocity* and *Ego Status MLP* as the lower bound for comparison. *Constant Velocity* model assumes constant speed from the current timestamp for forward movement. *Ego Status MLP* serves as a bind driving agent, which leverages a MLP for trajectory prediction given only the ego vehicle status.

Implementation Details. Our code is built on the PyTorch lightening framework [46] and official NAVSIM toolkit [43]. We take 10 timesteps during denoising process for both training and inference. The trade-off coefficient β in Eq. 4 is fixed to 0.02. The learning rate is set to $1e-4$, and global batchsize is 256, distributed across 4 NVIDIA[®] H20 GPUs. Adam optimizer [47] is adopted with OneCycle scheduler. As the task requires, the model outputs 8 waypoints spanning 4 seconds. Total training lasts for 120 epochs.

Metrics. For NAVSIM dataset, we evaluate our models based on the popular close-looped Predictive Driver Model score (PDMS [48]) which quantifies driving capacity by aggregating sub-metrics for multiple objectives such as progress and comfort. It can be formulated as follows:

$$PDM_{score} = NC \times DAC \times TTC \times \frac{(5 \times DDC + 2 \times C + 5 \times EP)}{12}, \quad (5)$$

where NC , DAC , TTC , C , EP , DDC correspond to the No at-fault Collisions, Drivable Area Compliance, Time to Collision, Comfort, Ego Progress, and Driving Direction Compliance. Note that DDC is exempted from calculation due to the practical constraints of the NAVSIM toolkit³. Following [16, 9], top-1 scoring predicted trajectory for each sample is used for PMDS evaluation. To measure the diversity of all generated candidate trajectories for each sample, we refer to [16] for the *Diversity metric*, and further discuss in Section 4.2.

4.2 Main Experiments

Benchmark Performance. As Table 2 indicates, TransDiffuser achieves the best performance on Nav-test. Performance of other models are cited from the original papers. Hydra-MDP++ provides a base version and a large version by scaling up the image encoder from ResNet-34 [49] to V2-99 [50].

³<https://github.com/autonomousvision/navsim/issues/14>

Table 3: Experimental results for ablation and sensitivity study.

Component	Value	Metrics						
		$NC \uparrow$	$DAC \uparrow$	$EP \uparrow$	$TTC \uparrow$	$C \uparrow$	$PDMS \uparrow$	$Diversity \uparrow$
Timestep T	5	98.5	94.4	92.7	95.8	99.8	92.4	65.35
	10	99.4	96.5	94.1	97.8	99.4	94.9	70.02
	20	99.0	96.0	94.6	96.7	99.3	94.3	87.99
Batchsize B	32	98.8	94.6	92.9	96.1	99.9	92.7	65.60
	64	99.4	96.5	94.1	97.8	99.4	94.9	70.02
	128	98.9	95.4	91.7	97.0	99.0	92.9	69.08
Coefficient β	0	99.0	95.8	94.5	96.8	99.9	94.3	65.90
	0.02	99.4	96.5	94.1	97.8	99.4	94.9	70.02
	0.05	99.0	95.9	93.8	97.2	99.3	94.1	69.26
	0.1	99.0	95.9	93.3	97.3	99.1	94.0	69.45

The most obvious improvement over previous works is the Ego Progress metric, which can also be intuitively observed in Figure 3. We can also witness the potential of Diffusion based models. Note that we do not require any anchor distributions or anchor trajectories as prior, discussed in Section 2.

Training Efficiency. Our training performs 120 epochs across four GPUs and consumes within 2 wall-clock hours. TransDiffuser model is about 251M parameters while the parameters of the perception encoder are frozen, thus only 62.8M parameters are trainable. Regarding inference-time efficiency, we discussed in Section 3.3.

Diversity Improvement. Following the diversity metric proposed and implemented in Diffusion-Drive [16], as shown in Table 3, we additionally measure the averaged *Diversity* metric of the generated trajectories of each sample over the test dataset. This measures the mean Intersection over Union (mIoU) between each denoised generated trajectory and the union of all denoised candidate trajectories for each sample. From the experimental results, we observe the existence of Multi-modal representation decorrelation regularization correspondingly improves the diversity of generated candidate trajectories (from 65.90 to 70.02).

4.3 Ablation & Sensitivity Study

Herein we study three key hyper-parameters: Diffusion timesteps T in Section 3.3, Batchsize B in Section 3.4 and β in Eq.3. As Table 3 indicates, our method shows robustness over the selection of coefficient β , diffusion timesteps T and batchsize B . We observe when we scale up the diffusion timesteps, the *Diversity* metric generally increases at the cost of more computation and latency, while small diffusion timesteps can also achieve satisfactory performance with higher efficiency.

4.4 Qualitative Analysis

We provide the visualization of representative examples from the BEV perspective. For simple traffic scenarios where there are less notable objects on the road, our framework can propose relatively more aggressive feasible planning trajectories. For complicated traffic scenarios where there are numerous notable objects around the ego driving agent, our framework tends to propose diverse yet feasible planning trajectories on the premise of ensuring safety.

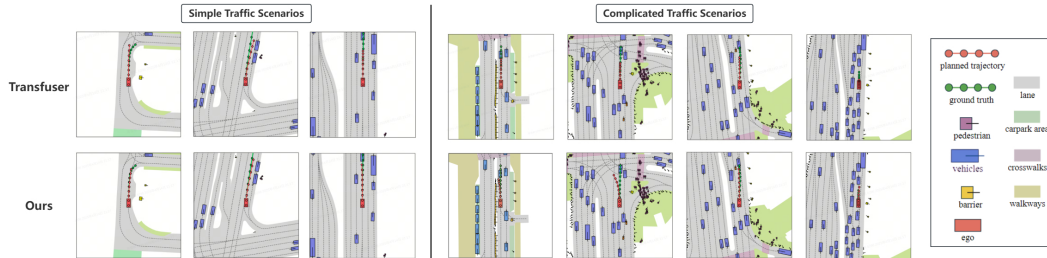


Figure 3: Visualization of representative examples of Transfuser [8] and our proposed framework.

5 Conclusion

In this work, we propose TransDiffuser, an encoder-decoder based generative trajectory model for end-to-end autonomous driving. The encoded scene features and motion features serves as conditional input of the Diffusion-based denoising decoder. We introduce a simple yet effective multi-modal representation decorrelation optimization mechanism to encourage more diverse trajectories from the continuous action space. Experiments on the planning-oriented NAVSIM benchmark demonstrate its superiority in generating high-quality diverse trajectories. For future works, considering more real-world autonomous driving scenarios, the autonomous vehicle should generate multiple planning trajectories better aligned with human driver commands or styles, these attempts may require reinforcement learning techniques [9] and vision-language-action model architectures [51, 52].

6 Limitations

In our experiments, we find there exists some difficulties when finetuning the full model (i.e. including the perception encoder), which requires more technical explorations to fully unleash the potential of the proposed framework. Future works can also consider applying our introduced plug-and-play decorrelation regularization on other models or try more advanced diffusion policies which may possibly improve the performance to enrich this study.

Acknowledgments

This work is a follow-up work of our team’s previous proposed TrajHF [9]. We sincerely appreciate the assistance of Jianwei Ren from Shanghai Qi Zhi Institute, along with Yue Wang, Chuan Tang and other engineers from LiAuto for TrajHF [9] re-implementation and other technical supports.

References

- [1] Y. Hu, J. Yang, L. Chen, K. Li, C. Sima, X. Zhu, S. Chai, S. Du, T. Lin, W. Wang, et al. Planning-oriented autonomous driving. In *Proceedings of the IEEE/CVF conference on computer vision and pattern recognition*, pages 17853–17862, 2023.
- [2] X. Tian, J. Gu, B. Li, Y. Liu, Y. Wang, Z. Zhao, K. Zhan, P. Jia, X. Lang, and H. Zhao. Drivevlm: The convergence of autonomous driving and large vision-language models. In *8th Annual Conference on Robot Learning*.
- [3] X. Jiang, F. Wang, R. Zheng, H. Liu, Y. Huo, J. Peng, L. Tian, and E. Barsoum. Vips-odom: Visual-inertial odometry tightly-coupled with parking slots for autonomous parking. *arXiv preprint arXiv:2407.05017*, 2024.
- [4] B. Liu, J. Tong, and Y. Zhuang. Edgeloc: A communication-adaptive parallel system for real-time localization in infrastructure-assisted autonomous driving. *arXiv preprint arXiv:2405.12120*, 2024.
- [5] H. Wang, H. Tang, S. Shi, A. Li, Z. Li, B. Schiele, and L. Wang. Unitr: A unified and efficient multi-modal transformer for bird’s-eye-view representation. In *Proceedings of the IEEE/CVF international conference on computer vision*, pages 6792–6802, 2023.
- [6] C. Pan, B. Yaman, T. Nesti, A. Mallik, A. G. Allievi, S. Velipasalar, and L. Ren. Vlp: Vision language planning for autonomous driving. In *Proceedings of the IEEE/CVF Conference on Computer Vision and Pattern Recognition*, pages 14760–14769, 2024.
- [7] A. Sadat, S. Casas, M. Ren, X. Wu, P. Dhawan, and R. Urtasun. *Perceive, Predict, and Plan: Safe Motion Planning Through Interpretable Semantic Representations*, page 414–430. Jan 2020. doi:10.1007/978-3-030-58592-1_25. URL http://dx.doi.org/10.1007/978-3-030-58592-1_25.

- [8] K. Chitta, A. Prakash, B. Jaeger, Z. Yu, K. Renz, and A. Geiger. Transfuser: Imitation with transformer-based sensor fusion for autonomous driving. *IEEE transactions on pattern analysis and machine intelligence*, 45(11):12878–12895, 2022.
- [9] D. Li, J. Ren, Y. Wang, X. Wen, P. Li, L. Xu, K. Zhan, Z. Xia, P. Jia, X. Lang, et al. Finetuning generative trajectory model with reinforcement learning from human feedback. *arXiv preprint arXiv:2503.10434*, 2025.
- [10] Z. Xing, X. Zhang, Y. Hu, B. Jiang, T. He, Q. Zhang, X. Long, and W. Yin. Goalflow: Goal-driven flow matching for multimodal trajectories generation in end-to-end autonomous driving. *arXiv preprint arXiv:2503.05689*, 2025.
- [11] B. Jiang, S. Chen, Q. Xu, B. Liao, J. Chen, H. Zhou, Q. Zhang, W. Liu, C. Huang, and X. Wang. Vad: Vectorized scene representation for efficient autonomous driving. In *Proceedings of the IEEE/CVF International Conference on Computer Vision*, pages 8340–8350, 2023.
- [12] S. Chen, B. Jiang, H. Gao, B. Liao, Q. Xu, Q. Zhang, C. Huang, W. Liu, and X. Wang. Vadv2: End-to-end vectorized autonomous driving via probabilistic planning. *arXiv preprint arXiv:2402.13243*, 2024.
- [13] Z. Li, K. Li, S. Wang, S. Lan, Z. Yu, Y. Ji, Z. Li, Z. Zhu, J. Kautz, Z. Wu, et al. Hydramdp: End-to-end multimodal planning with multi-target hydra-distillation. *arXiv preprint arXiv:2406.06978*, 2024.
- [14] K. Li, Z. Li, S. Lan, Y. Xie, Z. Zhang, J. Liu, Z. Wu, Z. Yu, and J. M. Alvarez. Hydramdp++: Advancing end-to-end driving via expert-guided hydra-distillation. *arXiv preprint arXiv:2503.12820*, 2025.
- [15] Z. Li, S. Wang, S. Lan, Z. Yu, Z. Wu, and J. M. Alvarez. Hydra-next: Robust closed-loop driving with open-loop training. *arXiv preprint arXiv:2503.12030*, 2025.
- [16] B. Liao, S. Chen, H. Yin, B. Jiang, C. Wang, S. Yan, X. Zhang, X. Li, Y. Zhang, Q. Zhang, et al. Diffusiondrive: Truncated diffusion model for end-to-end autonomous driving. *arXiv preprint arXiv:2411.15139*, 2024.
- [17] J. Ho, A. Jain, and P. Abbeel. Denoising diffusion probabilistic models. *Advances in neural information processing systems*, 33:6840–6851, 2020.
- [18] A. Z. Ren, J. Lidard, L. L. Ankile, A. Simeonov, P. Agrawal, A. Majumdar, B. Burchfiel, H. Dai, and M. Simchowitz. Diffusion policy policy optimization. *arXiv preprint arXiv:2409.00588*, 2024.
- [19] X. Weng, B. Ivanovic, Y. Wang, Y. Wang, and M. Pavone. Para-drive: Parallelized architecture for real-time autonomous driving. In *Proceedings of the IEEE/CVF Conference on Computer Vision and Pattern Recognition*, pages 15449–15458, 2024.
- [20] C. Sima, K. Chitta, Z. Yu, S. Lan, P. Luo, A. Geiger, H. Li, and J. M. Alvarez. Centaur: Robust end-to-end autonomous driving with test-time training. *arXiv preprint arXiv:2503.11650*, 2025.
- [21] Y. Li, Y. Wang, Y. Liu, J. He, L. Fan, and Z. Zhang. End-to-end driving with online trajectory evaluation via bev world model. *arXiv preprint arXiv:2504.01941*, 2025.
- [22] I. Goodfellow, J. Pouget-Abadie, M. Mirza, B. Xu, D. Warde-Farley, S. Ozair, A. Courville, and Y. Bengio. Generative adversarial networks. *Communications of the ACM*, 63(11):139–144, 2020.
- [23] D. P. Kingma, M. Welling, et al. Auto-encoding variational bayes, 2013.

- [24] J. Achiam, S. Adler, S. Agarwal, L. Ahmad, I. Akkaya, F. L. Aleman, D. Almeida, J. Altenschmidt, S. Altman, S. Anadkat, et al. Gpt-4 technical report. *arXiv preprint arXiv:2303.08774*, 2023.
- [25] A. Van Den Oord, S. Dieleman, H. Zen, K. Simonyan, O. Vinyals, A. Graves, N. Kalchbrenner, A. Senior, K. Kavukcuoglu, et al. Wavenet: A generative model for raw audio. *arXiv preprint arXiv:1609.03499*, 12, 2016.
- [26] J. Li, L. Hu, J. Zhang, T. Zheng, H. Zhang, and D. Wang. Fair text-to-image diffusion via fair mapping. *CoRR*, abs/2311.17695, 2023. doi:10.48550/ARXIV.2311.17695. URL <https://doi.org/10.48550/arXiv.2311.17695>.
- [27] H. Zhu, D. Tang, J. Liu, M. Lu, J. Zheng, J. Peng, D. Li, Y. Wang, F. Jiang, L. Tian, et al. Dip-go: A diffusion pruner via few-step gradient optimization. *Advances in Neural Information Processing Systems*, 37:92581–92604, 2024.
- [28] J. Li, L. Hu, Z. He, J. Zhang, T. Zheng, and D. Wang. Text guided image editing with automatic concept locating and forgetting. *arXiv preprint arXiv:2405.19708*, 2024.
- [29] S. Nie, F. Zhu, Z. You, X. Zhang, J. Ou, J. Hu, J. Zhou, Y. Lin, J.-R. Wen, and C. Li. Large language diffusion models. *arXiv preprint arXiv:2502.09992*, 2025.
- [30] T. Hua, W. Wang, Z. Xue, S. Ren, Y. Wang, and H. Zhao. On feature decorrelation in self-supervised learning. In *Proceedings of the IEEE/CVF international conference on computer vision*, pages 9598–9608, 2021.
- [31] Y. Shi, J. Liang, W. Zhang, C. Xue, V. Y. F. Tan, and S. Bai. Understanding and mitigating dimensional collapse in federated learning. *IEEE Trans. Pattern Anal. Mach. Intell.*, 46(5): 2936–2949, 2024. doi:10.1109/TPAMI.2023.3338063. URL <https://doi.org/10.1109/TPAMI.2023.3338063>.
- [32] X. Lu, P. Li, and X. Jiang. Fedlf: Adaptive logit adjustment and feature optimization in federated long-tailed learning. In *Asian Conference on Machine Learning*, pages 303–318. PMLR, 2025.
- [33] J. Li and H. Zhang. Sa-svd: Mitigating bias in face recognition by fair representation learning. In *2024 27th International Conference on Computer Supported Cooperative Work in Design (CSCWD)*, pages 471–476. IEEE, 2024.
- [34] X. Jiang, J. Li, N. Wu, Z. Wu, X. Li, S. Sun, G. Xu, Y. Wang, Q. Li, and M. Liu. Fnbench: Benchmarking robust federated learning against noisy labels. *Authorea Preprints*, 2024.
- [35] Y. Xue, K. Whitecross, and B. Mirzasoleiman. Investigating why contrastive learning benefits robustness against label noise. In *Proceedings of the 39th International Conference on Machine Learning*, volume 162 of *Proceedings of Machine Learning Research*, pages 24851–24871. PMLR, 17–23 Jul 2022. URL <https://proceedings.mlr.press/v162/xue22a.html>.
- [36] X. Jiang, P. Li, S. Sun, J. Li, L. Wu, Y. Wang, X. Lu, X. Ma, and M. Liu. Refining distributed noisy clients: An end-to-end dual optimization framework. *Authorea Preprints*, 2025.
- [37] H. Lee, K. Lee, D. Hwang, H. Lee, B. Lee, and J. Choo. On the importance of feature decorrelation for unsupervised representation learning in reinforcement learning. In *International Conference on Machine Learning*, pages 18988–19009. PMLR, 2023.
- [38] T. Chen, S. Kornblith, M. Norouzi, and G. Hinton. A simple framework for contrastive learning of visual representations. In *International conference on machine learning*, pages 1597–1607. PmLR, 2020.
- [39] J.-B. Grill, F. Strub, F. Altché, C. Tallec, P. Richemond, E. Buchatskaya, C. Doersch, B. Avila Pires, Z. Guo, M. Gheshlaghi Azar, et al. Bootstrap your own latent-a new approach to self-supervised learning. *Advances in neural information processing systems*, 33: 21271–21284, 2020.

- [40] S. Lin, C. Gao, J. Chen, S. Zhou, B. Hu, Y. Feng, C. Chen, and C. Wang. How do recommendation models amplify popularity bias? an analysis from the spectral perspective. In W. Nejdl, S. Auer, M. Cha, M. Moens, and M. Najork, editors, *Proceedings of the Eighteenth ACM International Conference on Web Search and Data Mining, WSDM 2025, Hannover, Germany, March 10-14, 2025*, pages 659–668. ACM, 2025. doi:10.1145/3701551.3703579. URL <https://doi.org/10.1145/3701551.3703579>.
- [41] A. Vaswani, N. Shazeer, N. Parmar, J. Uszkoreit, L. Jones, A. N. Gomez, Ł. Kaiser, and I. Polosukhin. Attention is all you need. *Advances in neural information processing systems*, 30, 2017.
- [42] R. A. Amjad and B. C. Geiger. Learning representations for neural network-based classification using the information bottleneck principle. *IEEE transactions on pattern analysis and machine intelligence*, 42(9):2225–2239, 2019.
- [43] D. Dauner, M. Hallgarten, T. Li, X. Weng, Z. Huang, Z. Yang, H. Li, I. Gilitschenski, B. Ivanovic, M. Pavone, et al. Navsim: Data-driven non-reactive autonomous vehicle simulation and benchmarking. *Advances in Neural Information Processing Systems*, 37:28706–28719, 2024.
- [44] S. Peng, K. Genova, C. Jiang, A. Tagliasacchi, M. Pollefeys, T. Funkhouser, et al. Openscene: 3d scene understanding with open vocabularies. In *Proceedings of the IEEE/CVF conference on computer vision and pattern recognition*, pages 815–824, 2023.
- [45] H. Caesar, J. Kabzan, K. S. Tan, W. K. Fong, E. Wolff, A. Lang, L. Fletcher, O. Beijbom, and S. Omari. nuplan: A closed-loop ml-based planning benchmark for autonomous vehicles. *arXiv preprint arXiv:2106.11810*, 2021.
- [46] W. A. Falcon. Pytorch lightning. *GitHub*, 3, 2019.
- [47] D. P. Kingma and J. Ba. Adam: A method for stochastic optimization. In *International Conference on Learning Representations (ICLR)*, 2015. URL <https://arxiv.org/abs/1412.6980>.
- [48] D. Dauner, M. Hallgarten, A. Geiger, and K. Chitta. Parting with misconceptions about learning-based vehicle motion planning. Jun 2023.
- [49] K. He, X. Zhang, S. Ren, and J. Sun. Deep residual learning for image recognition. In *2016 IEEE Conference on Computer Vision and Pattern Recognition (CVPR)*, Jun 2016. doi:10.1109/cvpr.2016.90. URL <http://dx.doi.org/10.1109/cvpr.2016.90>.
- [50] Y. Lee, J.-w. Hwang, S. Lee, Y. Bae, and J. Park. An energy and gpu-computation efficient backbone network for real-time object detection. In *2019 IEEE/CVF Conference on Computer Vision and Pattern Recognition Workshops (CVPRW)*, Jun 2019. doi:10.1109/cvprw.2019.00103. URL <http://dx.doi.org/10.1109/cvprw.2019.00103>.
- [51] M. J. Kim, K. Pertsch, S. Karamcheti, T. Xiao, A. Balakrishna, S. Nair, R. Rafailov, E. Foster, G. Lam, P. Sanketi, et al. Openvla: An open-source vision-language-action model. *arXiv preprint arXiv:2406.09246*, 2024.
- [52] J.-J. Hwang, R. Xu, H. Lin, W.-C. Hung, J. Ji, K. Choi, D. Huang, T. He, P. Covington, B. Sapp, et al. Emma: End-to-end multimodal model for autonomous driving. *arXiv preprint arXiv:2410.23262*, 2024.